Molecular Dynamics Simulations on the Effects of Diameter and Chirality on Hydrogen Adsorption in Single Walled Carbon Nanotubes

Hansong Cheng,*,† Alan C. Cooper,† Guido P. Pez,† Milen K. Kostov,‡ Pamela Piotrowski,§ and Steven J. Stuart*,§

Air Products and Chemicals, Inc., 7201 Hamilton Boulevard, Allentown, Pennsylvania 18195-1501, Department of Physics, The Pennsylvania State University, University Park, Pennsylvania 16802-6300, and Department of Chemistry, Clemson University, Clemson, South Carolina 29634

Received: October 11, 2004; In Final Form: January 11, 2005

We present systematic molecular dynamics simulation studies of hydrogen storage in single walled carbon nanotubes of various diameters and chiralities using a recently developed curvature-dependent force field. Our main objective is to address the following fundamental issues: 1. For a given H_2 loading and nanotube type, what is the H_2 distribution in the nanotube bundle? 2. For a given nanotube type, what is the maximal loading (H_2 coverage)? 3. What is the diameter range and chirality for which H_2 adsorption is most energetically favorable? Our simulation results suggest strong dependence of H_2 adsorption energies on the nanotube diameter but less dependence on the chirality. Substantial lattice expansion upon H_2 adsorption was found. The average adsorption energy increases with the lowering of nanotube diameter (higher curvature) and decreases with higher H_2 loading. The calculated H_2 vibrational power spectra and radial distribution functions indicate a strong attractive interaction between H_2 and nanotube walls. The calculated diffusion coefficients are much higher than what has been reported for H_2 in microporous materials such as zeolites, indicating that diffusivity does not present a problem for hydrogen storage in carbon nanotubes.

I. Introduction

One of the drivers for the incipient hydrogen economy is the continuing development of proton exchange membrane (PEM) fuel cells. Efficient hydrogen storage technologies are critical for the projected use of PEM fuel cells for power generation. Several recent experiments have suggested that single walled carbon nanotubes (SWNT) are capable of storing hydrogen at ambient temperature and moderate to high hydrogen pressures, although the reported storage capacity varies widely depending on the quality of the nanotubes and the pretreatment of the samples.[1−4] Of fundamental importance is the reported heat (enthalpy) of adsorption (∼4.5 kcal/mol),[1,2] which is strikingly higher than what has been found in graphitic carbons, such as graphite and activated carbons (0.9−1.25 kcal/mol)[5−9] and even graphite intercalation compounds (∼2.3 kcal/mol for KC_{24}).[10−13] The current consensus appears to be that the high enthalpy of H_2 adsorption on SWNT is related to the curvature of the graphitic walls of the nanotubes.[14] Nevertheless, many fundamental issues related to the effects of curvature and chirality and how these give rise to the strong H_2 adsorption enthalpy in SWNT remain to be addressed in detail in order to develop a comprehensive understanding of the overall adsorption phenomenon. First, for a given H_2 loading and nanotube type (diameter and chirality), how are the H_2 molecules distributed in the SWNT lattice? The ratio of endohedral/exohedral H_2 population in the lattice is largely determined by the energetics associated with adsorption in these sites. This requires careful examination of the various H_2 population distributions in the nanotube bundle. Second, for a given nanotube type (i.e., diameter and chirality), what is the highest possible H_2 loading? Is the gravimetric capacity target of 6.5 wt % H_2 set by the U.S. Department of Energy achievable? Finally, are there a range of SWNT diameters and/or a specific chirality for which H_2 adsorption is energetically most favorable? In this paper, we report our progress toward addressing these fundamental issues.

In previous publications,[15−17] we demonstrated using ab initio molecular dynamics based on local density functional theory that H_2 adsorption energies in a lattice of (9,9) armchair SWNT at a variety of temperatures with 0.4 wt % hydrogen loading are significantly higher than in graphite and graphite intercalation compounds. Despite the overbinding expected from local density functional theory calculations, the calculated adsorption energies were in a close proximity to a reported experimental value.[1,2] The simulation showed that H_2 adsorption in SWNT is a highly dynamic phenomenon with very high H_2 mobility in the lattice and substantial SWNT framework deformation at moderate temperatures. Consequently, it is crucial to model hydrogen adsorption at finite temperatures, with models that are capable of modeling the deformation of the SWNT walls. Unfortunately, ab initio molecular dynamics simulations are computationally expensive and thus cannot be used to achieve the objectives set in the present research. Subsequently, we developed an empirical force field scheme to describe molecular interactions in a curved carbon environment to allow large scale, long time molecular dynamics simulations.[18] The basic idea we considered was to explore the interactions of H_2 with SWNT in the range between two extreme diameters: SWNT with an infinite radius (i.e., graphene, a single layer of graphite) and SWNT with one of the smallest possible radii, the (2,2) armchair SWNT. In the latter case, the carbon atoms are extremely reactive and they individually behave like a carbon-based radical

* To whom correspondence should be addressed. E-mail: (H.C.) chengh@apci.com; (S.J.S.) ss@clemson.edu).
† Air Products and Chemicals, Inc.
‡ The Pennsylvania State University.
§ Clemson University.

10.1021/jp045358m CCC: $30.25
Published on Web 02/12/2005

with high reactivity,[19] while in the former case only a very weak interaction between H_2 and graphite is observed. It is therefore anticipated that a nanotube with a radius between these extremes would respond to H_2 uptake with a stronger interaction than graphite but with a weaker force than the smallest SWNT and that the intensity of the interaction would depend on the diameter of the nanotube. A carbon atom in a highly curved carbon surface readily adopts a pseudotetrahedral configuration, resulting in high electron density on the exterior surface of the SWNT.[15,18] Will this give rise to the preferential adsorption of H_2 in the interstitial sites of the SWNT bundles rather than inside the nanotubes (endohedral sites)? Will the endohedral sites be populated with a significant H_2 loading via van der Waals forces?

Using this force field developed specifically for molecular adsorption on curved carbon surfaces, we performed extensive classical molecular dynamics simulations to address the most fundamental issues of hydrogen storage in single walled carbon nanotubes outlined at the beginning of this paper. The nanotubes chosen in this study include three armchair, three zigzag, and one with chiral structure, with a range of diameters. Hydrogen adsorption in these nanotubes at ambient temperature with loadings ranging from 0.4 to 6.5 wt % was systematically investigated. The average heats of H_2 adsorption in all cases were evaluated to gain understanding of the ambient-temperature hydrogen storage feasibility.

II. Computational Details

The results of molecular dynamics simulations are critically dependent on the quality of the force field. In principle, all energy terms defined in a force field for SWNT should be curvature dependent. However, the curvature effect has not been properly accounted for in force fields published in the literature.[20−23] In particular, the nonbonding interaction terms, which most sensitively affect the calculated adsorption energies, have been made completely independent of nanotube curvature. In fact, for most of these force fields, the potential parameters were derived from sp^2 hybridized graphitic carbons (an infinite-radius SWNT). It is conceivable that the bonding interactions in SWNT may not be very sensitive to the nanotube curvature. In fact, the experimental structures as well as the vibrational spectra for some of the SWNT systems were well reproduced with some common force fields[20,22] because these properties depend primarily on intratube carbon−carbon interactions. However, to describe hydrogen adsorption in SWNT accurately, the nonbonding interactions, and in particular the H−C interactions, must be made curvature dependent.

To include curvature dependence in both the covalent and nonbonding interactions, we used the adaptive intermolecular reactive bond-order (AIREBO) potential,[24] with modified van der Waals interactions. This potential uses the same bonding interactions as the well-known Brenner REBO potential[25,26] and correctly accounts for local curvature dependence in the covalent bonding interactions. Thus, this potential is able to correctly treat chemisorption, should that occur. However, the original potential does not include any curvature dependence in the Lennard-Jones (L-J) parameters used to describe the nonbonded van der Waals interactions (physisorption). Consequently, we modified the Lennard-Jones parameters, based on the curvature of the nanotube.

The van der Waals interaction was refit for H_2 adsorption in SWNT by first fitting the L-J parameters for H−H interactions to the recent high level ab initio results on interactions between H_2 molecules reported by Diep and Johnson,[27] yielding a center of mass separation of 3.4 Å, and the Lennard-Jones parameters $\sigma_{HH} = 2.65$ Å and $\epsilon_{HH} = 17.4$ K. For the nonbonding interaction between carbon atoms, we anticipate that this will not have a pronounced effect on the H_2 adsorption energy and thus still use the standard AIREBO potential parameters of $\sigma_{CC} = 3.40$ Å and $\epsilon_{CC} = 33.0$ K.

TABLE 1: Lennard-Jones Parameters for sp^2 and sp^3 Carbons Used for Nonbonding Interactions[a]

	ϵ_{C-C}	σ_{C-C}	ϵ_{C-H} (end)	ϵ_{C-H} (exo)
sp^2	2.410	3.40	2.24	2.24
sp^3	2.340	3.57	4.00	11.0

[a] Units: σ in Å and ϵ in meV.

For the interaction potential between H_2 and carbon atoms, we introduce a new procedure to derive the Lennard-Jones parameters from the existing force fields for interatomic potential functions for carbon atoms with sp^2 and sp^3 hybridizations, which have been developed using either experimental or ab initio results. The L-J parameters σ and ϵ are made explicitly dependent on the radius of the nanotube, r, using the following equations:

$$\sigma(r) = f(r)\sigma_{sp^2} + [1 - f(r)]\sigma_{sp^3} \quad (1)$$

$$\epsilon(r) = \begin{cases} f(r)\epsilon_{sp^2} + [1 - f(r)]\epsilon_{sp^3}^{exo} & \text{exohedral} \\ f(r)\epsilon_{sp^2} + [1 - f(r)]\epsilon_{sp^3}^{end} & \text{endohedral} \end{cases} \quad (2)$$

where $f(r) = (1 - r_0/r)^{\lambda}$ and $r_0 = 1.356$ Å is the radius of a (2,2) nanotube, assumed to demonstrate purely sp^3 bonding. The nonbonding interactions in a nanotube with a large radius will be similar to those in a graphite sheet while these interactions can be substantially enhanced in small radius nanotubes, as $\epsilon_{sp^3} > \epsilon_{sp^2}$. In the present work, we chose λ to be 0.62 so that the van der Waals surface of an endohedral H_2 aligned along the axis of a (m,n) nanotube touches the van der Waals surface of the SWNT wall. This procedure can be used to derive curvature-dependent L-J parameters from curvature-independent values of σ and ϵ. The specific parameters used in this study, which are obtained from previous ab initio calculations,[14] are shown in Table 1. Because the σ_{C-H} parameter is essentially insensitive to the SWNT curvature, varying by only 2.0% from sp^2 to sp^3 carbon, we chose a single value of $\sigma_{C-H} = 2.78$ Å for both sp^2 and sp^3 carbon. The strength of the interaction varies considerably, however, both with hybridization and direction of curvature, as illustrated by the variation of values of ϵ_{C-H} in Table 1. The detailed fitting procedure can be found in ref 18.

Using this curvature-dependent force field, we have carried out extensive MD simulations of H_2 adsorption and storage in SWNT. In contrast to all previously published classical simulations, the potential well depth between H and C atoms for exohedral adsorption is now treated differently from that for endohedral adsorption. Our MD simulations were conducted in the constant-*NVT* canonical ensemble using the Langevin thermostat, at ambient temperature of 300 K. For a given SWNT, periodic boundary conditions were applied via a rectangular box containing $1 \times 2 \times 10$ primitive cells of the SWNT. The equations of motion were integrated using the velocity Verlet algorithm with a time step of 0.25 fs. The Lennard-Jones potential was switched off smoothly at 3σ using a cubic spline, and long-range corrections were applied to the system energy. All systems were first structurally minimized and then equilibrated at 300 K for times ranging from 10 to 30 ps. For a given H_2 loading, nanotube type and H_2 distribution (the percentage of H_2 molecules at the endohedral/exohedral

TABLE 2: Calculated Optimal Distribution of H_2 and the Average Adsorption Energy (kcal/mol) per H_2[a]

		0.4 wt % H_2 loading		3.0 wt % H_2 loading		6.5 wt % H_2 loading	
nanotube (n,m)	SWNT diameter (Å)	endo/exo ratio	ΔE_{ad} (kcal/mol)	endo/exo ratio	ΔE_{ad} (kcal/mol)	endo/exo ratio	ΔE_{ad} (kcal/mol)
(3,3)	4.068	0:100	5.7	0:100	4.9	0:100	3.7
(5,5)	6.780	0:100	5.1	20:80	2.4	30:70	1.7
(9,9)	12.204	0:100	3.8	40:60	1.4	50:50	1.1
(5,0)	3.914	0:100	5.3	0:100	5.1	0:100	2.8
(10,0)	7.828	0:100	4.8	20:80	2.1	30:70	0.9
(15,0)	11.743	0:100	3.3	30:70	1.1	50:50	0.6
(8,4)	8.285	0:100	4.3	20:80	1.9	30:70	0.6

[a] The uncertainty of the averaged adsorption energy is approximately ±0.5 kcal/mol.

sites), the H_2 molecules were initially placed randomly in the lattice but significantly away from the nanotube walls to avoid chemisorption. The total simulation time after equilibration was 100 ps for each system. The total energy for each MD run is obtained by averaging the sum of potential energies in the entire simulation course and then utilized to define the adsorption energy using eq 3.

$$\Delta E_{ad} = E_{tube+H_2} - E_{tube} - E_{H_2} \quad (3)$$

The H_2 vibrational power spectrum was obtained from the Fourier transform of the hydrogen velocity autocorrelation functions.

III. Results and Discussion

The SWNT systems chosen in the present studies include three armchair nanotubes and three zigzag nanotubes with diameters ranging from 4 to 12 Å, and one chiral nanotube with a diameter of 8.28 Å. The nanotubes were carefully chosen to address the following fundamental issues. First, to understand the curvature effect on hydrogen uptake, we selected nanotubes with diameters varying from about 4 to 12 Å. Next, to investigate the effect of nanotube chirality, we intentionally chose the nanotubes of different chiral architectures with similar diameters. Finally, to study the capacity of a given nanotube, we included three different H_2 loadings at 0.4, 3.0, and 6.5 wt %, respectively, in our MD simulations.

In the simulations with the highest H_2 loading of 6.5 wt %, the lattice constants of the periodic lattice were adjusted independently during the equilibration process in order to reduce the diagonal components of the pressure tensor toward ambient pressure. Substantial lattice expansion upon H_2 uptake was observed, particularly for the smaller diameter nanotubes. This is expected because a higher hydrogen loading requires a larger interstitial pore volume to accommodate the H_2 molecules. The volume of both exohedral and endohedral sites decreases as the nanotube diameter becomes smaller. In no case was the system volume allowed to surpass twice the unloaded volume, thus providing a limit on the lattice swelling. Consequently, the 6.5 wt % simulations were performed at higher than ambient pressure, ranging from 7500 bar for the (3,3) tube with 4.1 Å diameter down to ~1000 bar for the (15,0) tube with 11.8 Å diameter. These elevated pressures even at near 100% lattice dilation suggest that hydrogen adsorption at the DOE target of 6.5 wt % presents difficulties.

III.1. H_2 Distribution in SWNT Bundle. To obtain accurate estimates of adsorption energies, it is important to understand how H_2 molecules are distributed in the lattice of each SWNT type. Specifically, for a given nanotube type and H_2 loading, we must first determine the ratio of H_2 adsorption at the endohedral sites vs the exohedral sites. Because of the extremely high barrier to passage through the nanotube wall, it is impossible for any H_2 molecule to migrate from an endohedral site to the exohedral site and vice versa. We therefore performed a series of simulations to determine the H_2 distribution at these sites. It is reasonable to assume that the distribution is dictated by the adsorption thermodynamics and that entropic effects arising from differences in pore geometry and free pore volume are negligible. That is, the free energy can be approximated by the internal energy. This approximation will be most accurate when the free volume is similar in the endohedral and exohedral pores, as will be the case for high loadings and for near-optimal hydrogen distributions. Thus, we assume that the ratio corresponding to the highest average heat of adsorption represents the thermodynamically most favorable distribution. For each nanotube type, we sampled the endohedral/exohedral ratio with distributions ranging from 100% endohedral to 100% exohedral, in steps of 10%, to search for the optimal distribution of H_2 in the SWNT bundles. The calculated optimal H_2 distributions and the adsorption energies are shown in Table 2.

At 0.4 wt % loading, H_2 molecules are found to be exclusively adsorbed in the interstitial space in all cases. The recent experiments conducted by Shiraishi et al.[2] suggested that the hydrogen, which is adsorbed at ambient temperature under high hydrogen pressure (9 MPa) and subsequently desorbed at near-ambient temperatures under vacuum at 0.3 wt % loading, is physisorbed in the exohedral sites. Our results are consistent with their findings. As the H_2 loading increases, the endohedral sites in nanotubes with larger diameters become populated due to competing effects. The curvature of nanotubes clearly gives the exohedral adsorption an advantage but an excessive population at the exohedral sites will push the H_2-H_2 interactions into the repulsive region. The endohedral adsorption, on the other hand, would allow the H_2 molecule to effectively interact with more carbon atoms but with a weaker pair interaction force. As a consequence, the exohedral sites will be filled first upon H_2 uptake and subsequently the endohedral sites will be populated when the interstitial space of the nanotube bundles becomes saturated with hydrogen. It is worth noting that the H_2 adsorption in the two smallest diameter nanotubes, (3,3) and (5,0), is exclusively exohedral because the exceedingly small diameters cause overly close contacts between the H_2 molecules and the nanotube wall at the endohedral sites and force the interaction to fall into the repulsive region. The general trend of the H_2 population distribution in the SWNT bundles is that the population at the endohedral sites increases with the H_2 loading and/or the nanotube diameters with no apparent preference for the chirality observed.

III.2. Heat of Adsorption. The calculated average heats of adsorption at room temperature are shown in Table 2. These results indicate that the heat of adsorption increases as the nanotube diameter decreases. This is consistent with the observation that the curvature of small nanotubes is greater and thus the carbon hybridization, as determined by C−C−C bond

angles, is more consistent with sp^3, leading to a stronger interaction with H_2. Of course, this result should be expected since the stronger H_2 interaction with smaller nanotubes are built into the force field. Shiraishi et al. recently reported an experimentally measured heat of adsorption of 4.84 kcal/mol with a loading of 0.3 wt % H_2 in SWNT of ca. 1.4 nm diameter.[2] Our calculated heats of adsorption energies for SWNT of similar diameter and H_2 loading are in good agreement with their experimental results.

Furthermore, the calculated average heat of adsorption decreases as the H_2 loading increases. In particular, at the DOE gravimetric density target of 6.5 wt % H_2, the heat of adsorption decreases substantially relative to lower loadings. This trend is consistent with our previous ab initio MD studies.[15] Detailed analysis of the MD trajectories at 6.5 wt % loading indicates that H_2 molecules form a double layered structure at the endohedral sites in the larger tubes, and that the exohedral sites have a high density of H_2, with considerable lattice dilation. As a consequence, the H_2 molecules that reside at short distances from the nanotube walls interact strongly with SWNT bundles and those with large distances from the walls experience only a very small attraction from the nanotube walls, reducing the average heat of adsorption. In addition, the reduction of heat of adsorption can also be attributed partly to the large repulsive forces among H_2 molecules under compression. Only the smallest nanotubes with a diameter close to 4 Å show significant adsorption energies for H_2 at 6.5 wt % H_2 loading. The average heat of adsorption decreases when the H_2-H_2 repulsion is strong (at high pressure, i.e., high loading), when the H_2−SWNT distance is large (at high loading and large SWNT radius) and when the H_2−SWNT interaction is weak (at large SWNT radius).

It is important to emphasize that H_2 adsorption is a highly dynamic and chaotic phenomenon. As such, H_2 molecules do not reside at a specific site permanently (except that they cannot migrate from the endohedral sites to the exohedral sites and vice versa). Instead, they move constantly from locations close to the SWNT walls to areas within the pores away from the walls. For exohedral adsorption, due to the lattice dilation, H_2 molecules can even readily migrate from one channel to another. The barrier for such movement between exohedral pores at room temperature is very low.

III.3. Radial Distribution Functions. Figure 1 displays the calculated radial distribution functions of H_2 adsorbed in a number of types of SWNT at 6.5 wt % loading. The feature at ca. 0.74 Å in Figure 1a corresponds to a H−H bond distance that is somewhat broadened compared to gas-phase H_2 at 300 K. A fraction of the H_2 molecules have a H−H bond that is elongated, resulting from the attractive interaction with SWNT walls; others have shorter H−H distances, largely due to the H_2-H_2 repulsion at high hydrogen density. Figure 1b represents the intermolecular distance between H_2 molecules. The first peak occurs at H−H distances of between 2.7 and 3.0 Å for different systems, primarily reflecting the difference in H_2 density. A substantial fraction of the first peak occurs at H−H separations below $\sigma_{HH} = 2.65$ Å, indicating that there is significant H−H repulsion, leading to much of the reduction in H_2 adsorption enthalpy at 6.5 wt % loading.

Figure 2 shows the radial distribution function for C−H distance during simulation of hydrogen adsorption in the various types of SWNT. The sharp rise near 2 Å represents the distance of closest approach of H_2 molecules to the SWNT, demonstrating purely physisorption behavior. Once again, there is substantial density below $\sigma_{C-H} = 2.78$ Å, reflecting the high H_2 density at this loading. The variation in distance of closest approach is somewhat surprising, however, and does not directly track the system pressure (or tube radius). The H_2 molecules remain the largest distance away from the smaller (3,3) and (5,0) tubes, despite these being at the largest pressures, and they approach most closely to the intermediate-radius tubes.

III.4. H_2 Vibrational Power Spectrum. From the calculated MD trajectories, we calculated autocorrection functions for the hydrogen velocities and Fourier transformed them to obtain the vibrational power spectrum. Figure 3 displays the calculated H_2 vibrational power spectrum for various SWNT bundles at 6.5 wt % H_2 loading. The feature around 4250 cm^{-1}, which is close to the calculated gas-phase value for the H−H stretching frequency, corresponds to the H−H stretching frequency of the hydrogen adsorbed in SWNT. The H−H frequencies of the hydrogen adsorbed in SWNT are significantly broadened compared with the gas-phase frequencies, which is another indication of the wide variation in H_2 environments—both interacting strongly with the SWNT and compressed by the high densities. The peak position is largely unchanged in different SWNTs, however. Contrary to previous studies with similar potentials at very low loading,[26] we see no evidence of a systematic red-shift in the H_2 vibrational frequency upon adsorption, which is likely due to the large loading of H_2 that gives rise to significant H_2-H_2 repulsion in addition to H_2−SWNT attractive interactions.

III.5. H_2 Diffusion Coefficients in SWNT. From the MD trajectories, we calculated the H_2 diffusion coefficients at 6.5 wt % loading in the nanotube bundles. The diffusion coefficients were evaluated from the limiting slope of the mean square displacement (MSD) curve with time (excluding both the initial, transient ballistic motion as well as the statistically noisy final region). The mean square displacement was calculated separately in the longitudinal (z) direction and the lateral (x and y) directions, as either $^1/_2$ or $^1/_4$ the slope of the MSD curve, respectively. The results are summarized in Table 3. The lateral diffusion coefficients are nonzero, because of the possibility of migration between interstitial pores. Indeed, the lateral diffusion coefficient is quite large, considering that it includes contributions from the endohedral H_2 molecules that do not diffuse laterally. The longitudinal diffusion coefficient is even larger, in all but one of the systems, although there appears to be no correlation with nanotube radius, H_2 density, or chirality. A large diffusion coefficient is advantageous, as it assists in the loading and unloading of H_2 during the duty cycle of the material. Consequently, it is a strong selling point for SWNT as H_2 storage materials that the calculated H_2 diffusion coefficients in SWNT appear much larger than what those that are typically found in microporous materials such as zeolites.[28−30] Nevertheless, the calculated diffusion coefficients are still much smaller (about 3−10 times) than what was reported in a recent equilibrium molecular dynamics study by Skoulidas et al.[31] A number of differences in the simulation methodology could be responsible for this. The potential parameters used in their simulations were derived from fluid−graphite interactions, and the nanotubes were kept rigid during the entire simulation. Thermal fluctuation in the SWNT walls, already observed to be important in previous ab initio molecular dynamics simulations,[15] will act to decrease the diffusion coefficient. In addition, while the interaction of H_2 with planar graphitic surfaces is quite weak, and should thus lead to fast diffusion, the stronger interactions with curved SWNT surfaces in the current curvature-dependent force field will also act to reduce the diffusivity.

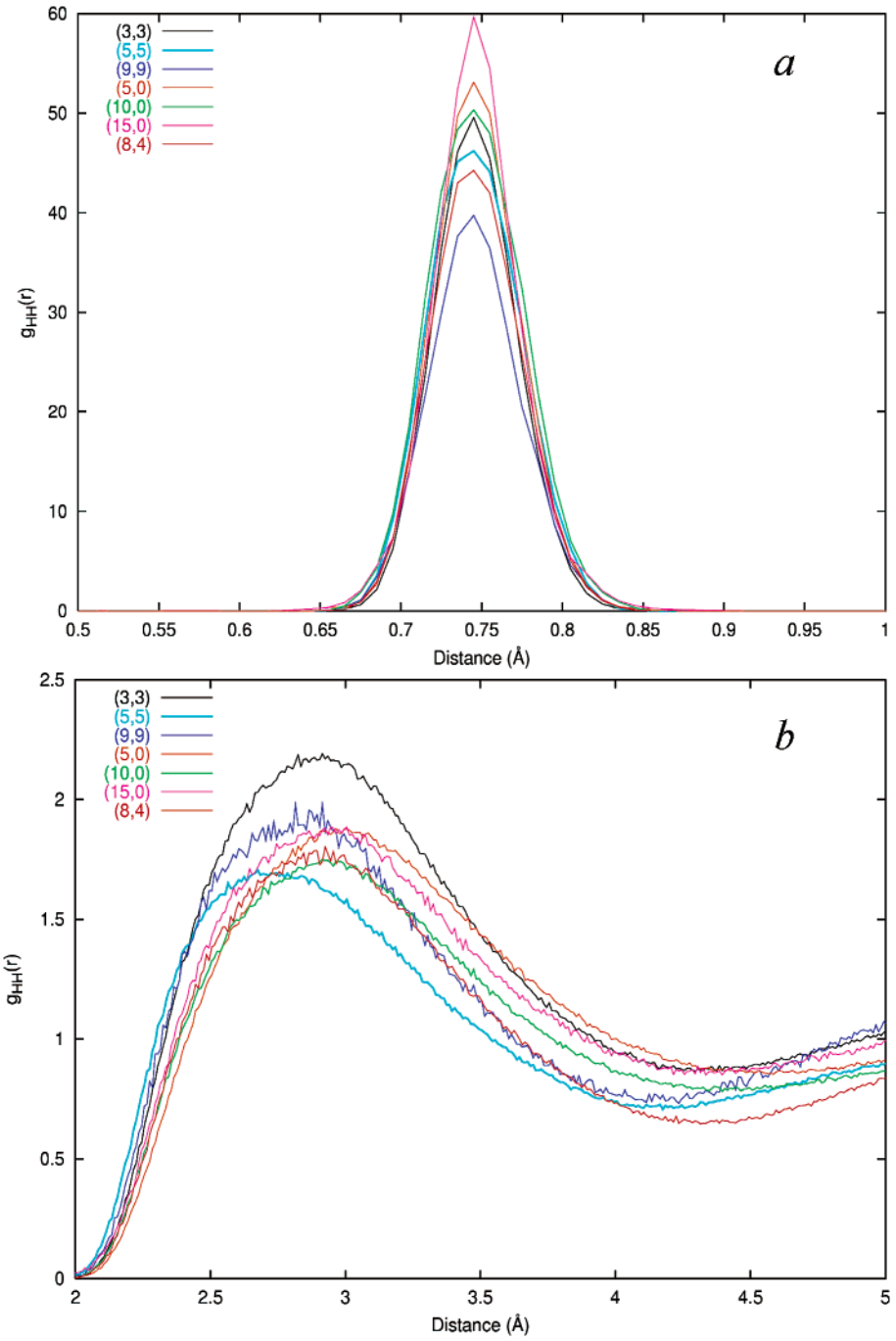

Figure 1. Radial distribution function for H−H separations: (a) intramolecular distance; (b) intermolecular distance.

Finally, the elevated pressures in the current study will also decrease the diffusion coefficient.

IV. Conclusions

Single walled carbon nanotubes have shown some promise to be a viable adsorbent for hydrogen storage. However, many fundamentally important issues have remained unanswered. In this paper, we have attempted to address some of these issues by performing a series of molecular dynamics simulations using a recently developed curvature-dependent force field. Our main objective was to explore several important aspects of H_2 adsorption in SWNT with diameters ranging from 4 to 12 Å. We have found that the H_2 distribution in the various nanotube lattices varies significantly with the nanotube diameter and H_2 loading. For low H_2 densities, H_2 tends to adsorb in the exohedral sites. As the H_2 loading increases, the endohedral sites become more populated. The larger the nanotube diameter, the higher the relative population in the endohedral sites. However, the population at the endohedral sites never exceeds 50% of the total adsorbed H_2 for tubes up to 12 Å in diameter. The calculated heats of adsorption for H_2 in larger diameter nanotubes at low H_2 loading are in good agreement with the reported experimental data. The H_2 adsorption energy increases as the nanotube diameter decreases. It was found that substantial SWNT lattice dilation could occur upon H_2 adsorption and that high adsorbed H_2 densities increase repulsion among H_2 molecules, giving rise to lower adsorption energies. For H_2 loading at 6.5 wt %, it was found in the calculated radial distribution functions for H−H distance that the average H−H bond length are slightly broadened around its gas-phase value.

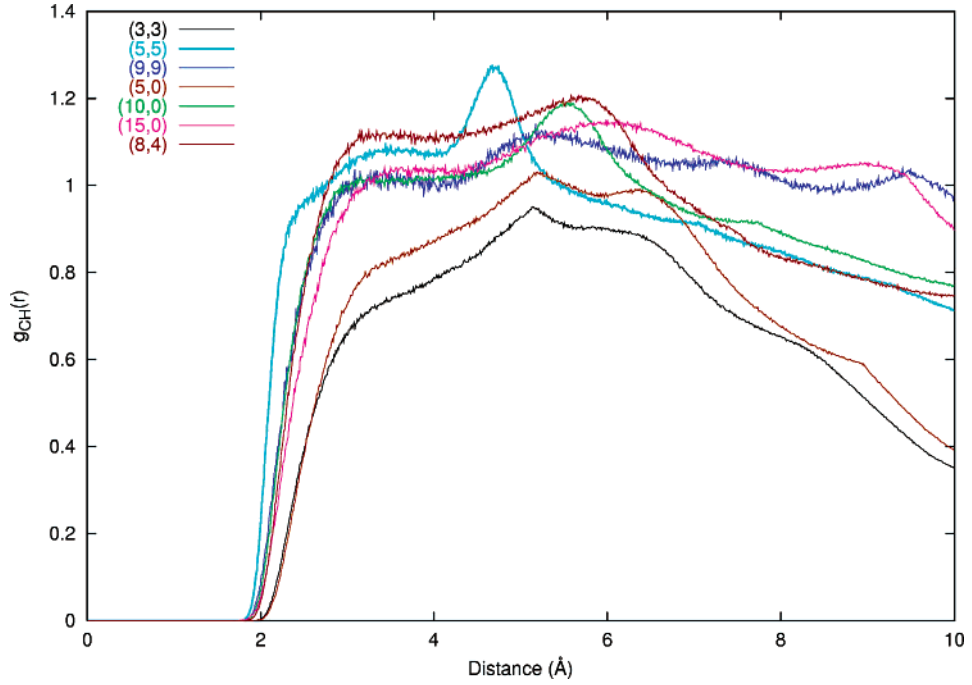

Figure 2. Radial distribution function for C−H separations.

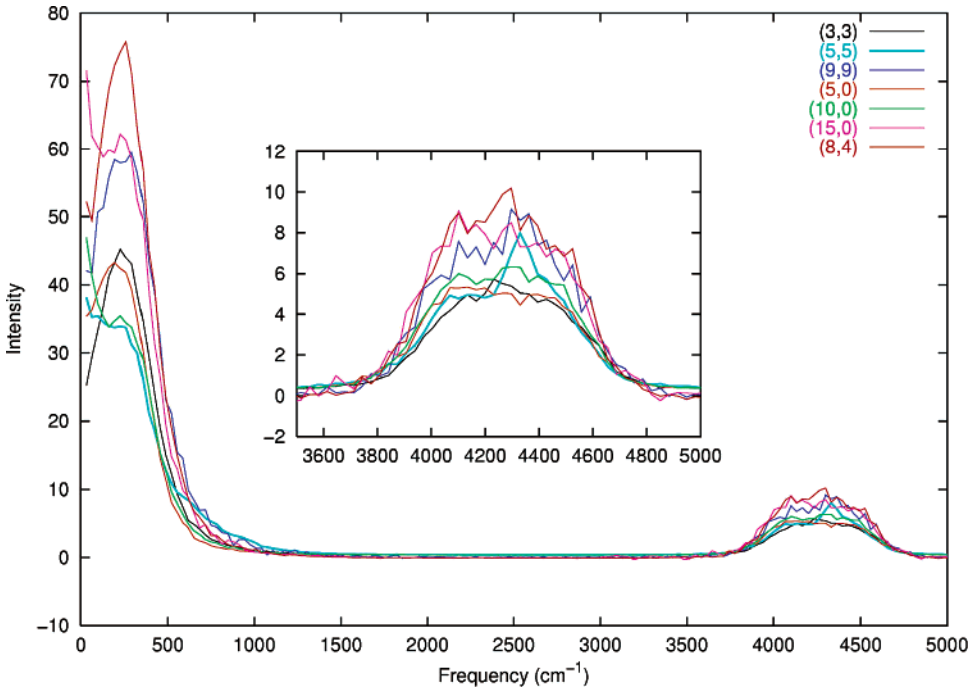

Figure 3. H_2 vibrational power spectra.

TABLE 3: Calculated H_2 Diffusion Coefficients in SWNT Bundles (Unit: 10^{-5} cm^2/s)

	(3,3)	(5,5)	(9,9)	(5,0)	(10,0)	(15,0)	(8,4)
diameter (Å)	4.07	6.78	12.20	3.91	7.83	11.74	8.29
lateral	27.3	35.3	40.9	28.8	62.2	54.8	36.2
longitudinal	29.2	100.1	31.5	65.5	92.4	61.7	57.5

The bond lengthening corresponds to a significant attractive interaction between H_2 and SWNT, while the bond compression can be attributed mostly to H_2-H_2 repulsions. The attractive interaction occurs when H_2 molecules approach the nanotube walls at a distance of around 3 Å. Strong H_2-H_2 repulsions take place when the H_2 is away from the SWNT walls. This conclusion is also clearly supported by the calculated H_2 vibrational power spectra, which show a very broad feature around the gas-phase H_2 stretching frequency. Given the fact that the practically acceptable heat of adsorption is found only for very small carbon nanotubes at 6.5 wt % loading, we conclude that it would be difficult to reach the DOE target with the SWNT with a diameter larger than 6 Å. Finally, the calculated diffusion coefficients for H_2 in SWNT are much larger than what has been reported in microporous materials such as zeolites and have been calculated with less limiting assumptions than in previous simulations,[26] showing a superb transport property of SWNT as a promising H_2 storage material. In all cases, the behavior of H_2 in the SWNT systems is highly chaotic and SWNT lattices undergo substantial thermal deformation in the presence of adsorbed hydrogen.

In this paper, all SWNTs are treated with an infinite bundle of homogeneous nanotubes. Shi and Johnson recently showed that packing defects due to nanotube inhomogeneity that give rise to large interstitial channels in the lattice can be important for gas adsorption.[32] This effect is not discussed here. In addition, there are a number of issues related to the simulation technique that also need to be addressed in future studies. In Table 2, it is apparent that the H_2 adsorption energy of the armchair nanotubes appears to be slightly larger than that of the zigzag nanotubes of similar diameter. Although there are potentially differences in adsorption energy for tubes of different chirality, this specific result is likely an artifact resulting from the force field used in our calculations. The REBO[25,26] and AIREBO[24] force fields both fail to predict the correct relative stability of aromatic molecule analogues of armchair and zigzag nanotubes. For example, contrary to quantum-mechanical and experimental results, the AIREBO force field predicts the energy of phenanthrene (armchair) relative to anthracene (zigzag) to be about 1.9 kcal/mol at 298 K, while the experimental result, using measured heats of formation, is −7.1 kcal/mol.[33] Likewise, for SWNT of similar size, the AIREBO force field predicts that the zigzag architecture is more stable than the armchair. We have tested a number of other force fields available to us, such as CVFF, COMPASS, CFF95, MMFF94, Sybyl, etc., and found that, without exception, these force fields all predict the incorrect relative stability of armchair and zigzag aromatic structures. The fact that the zigzag nanotubes are in fact less stable than the armchair structures, as correctly predicted by quantum mechanical calculations, implies that H_2 adsorption should be stronger in the zigzag tubes than in the armchair tubes. We thus expect that the relative H_2 adsorption energies between zigzag and armchair tubes are the reverse of those shown in Table 2. We plan to refine the AIREBO force field in our future work to account for the strong chirality effect.

Acknowledgment. We are very grateful to Prof. Milton Cole for many useful discussions and for his support. S.J.S. gratefully acknowledges financial support for this work by the Department of Energy (DE-FG02-01ER45889) and the National Science Foundation (CHE-0239448).

Supporting Information Available: Tables of the initial coordinates of 6.5 wt % H_2 in the SWNT used in our MD simulations. This material is available free of charge via the Internet at http://pubs.acs.org.

References and Notes

(1) Dillon, A. C.; Jones, K. M.; Bekkedahl, T. A.; Kiang, C. H.; Bethune, D. S.; Heben, M. J. *Nature (London)* **1997**, *386*, 377.

(2) Shiraishi, M.; Takenobu, T.; Ata, M. *Chem. Phys. Lett.* **2003**, *367*, 633.

(3) Liu, C. Y.; Fan, Y.; Lu, M.; Cong, H. T.; Cheng, H. M.; Dresselhaus, M. S. *Science* **1999**, *286*, 1127.

(4) Ye, Y.; Ahn, C. C.; Witham, C.; Fultz, B.; Liu, J.; Rinzler, A. G.; Colbert, D.; Smith, K. A.; Smalley, R. E. *Appl. Phys. Lett.* **1999**, *74*, 2307.

(5) Pace, E.; Siebert, A. *J. Phys. Chem.* **1959**, *63*, 1398.

(6) Dericbourg, J. *Surf. Sci.* **1976**, *59*, 565.

(7) Constabaris, G.; Sams, J.; Halsey, G. *J. Phys. Chem.* **1961**, *65*, 367.

(8) Pez, G.; Steyert, W. U.S. Patent 4,580,404.

(9) Benard, P.; Chahine, R. *Langmuir* **2001**, *17*, 1950.

(10) Watanabe, K.; Soma, M.; Onishi, T.; Tamaru, K. *Nature (London)* **1971**, *233*, 160.

(11) Watanabe, K.; Kondow, T.; Soma, M.; Onishi, T.; Tamaru, K. *Proc. R. Soc. London, A* **1973**, *A333*, 51.

(12) Lagrange, P.; Metrot, A.; Herold, A. *C. R. Acad. Sci. Ser.* **1972**, *C275*, 765.

(13) Terai, T.; Takahashi, Y. *Synth. Met.* **1989**, *34*, 329.

(14) Okamoto, Y.; Miyamoto, Y. *J. Phys. Chem. B* **2001**, *105*, 3470.

(15) Cheng, H.; Pez, G. P.; Cooper, A. C. *J. Am. Chem. Soc.* **2001**, *123*, 5845.

(16) Canto, G.; Ordejon, P.; Cheng, H.; Cooper, A. C.; Pez, G. P. *New J. Phys.* **2003**, *5*, 124.1.

(17) Cheng, H.; Pez, G.; Kern, G.; Kresse, G.; Hafner, J. *J. Phys. Chem. B* **2001**, *105*, 736.

(18) Kostov, M. K.; Cheng, H.; Cooper, A. C.; Pez, G. P. *Phys. Rev. Lett.* **2002**, *89*, 146105-1.

(19) Cheng, H.; Pez, G. P.; Cooper, A. C. *Nano Lett.* **2003**, *3*, 585.

(20) Frankland, S. J. V.; Brenner, D. W. *Chem. Phys. Lett.* **2001**, *334*, 18.

(21) Wang, Q.; Johnson, J. K. *J. Chem. Phys.* **1999**, *110*, 577.

(22) Williams, K. A.; Eklund, P. C. *Chem. Phys. Lett.* **2000**, *320*, 352.

(23) Darkrim, F.; Levesque, D. *J. Chem. Phys.* **1998**, *109*, 4981.

(24) Stuart, S. J.; Tutein, A. B.; Harrison, J. A. *J. Chem. Phys.* **2000**, *112*, 6472.

(25) Brenner, D. W.; Shenderova, O. A.; Harrison, J. A.; Stuart, S. J.; Ni, B.; Sinnott, S. *J. Phys.: Condens. Matt.* **2002**, *14*, 783.

(26) Brenner, D. W. *Phys. Status Solidi B* **2000**, *217*, 23.

(27) Diep, P.; Johnson, J. K. *J. Chem. Phys.* **2000**, *112*, 4465.

(28) Skoulidas, A. I.; Sholl, D. S. *J. Phys. Chem. B* **2001**, *105*, 3151.

(29) Skoulidas, A. I.; Sholl, D. S. *J. Phys. Chem. B* **2002**, *106*, 5058.

(30) Maginn, E. J.; Bell, A. T.; Theodorou, D. N. *J. Phys. Chem.* **1993**, *97*, 5173.

(31) Skoulidas, A. I.; Ackerman, D. M.; Johnson, J. K.; Sholl, D. S. *Phys. Rev. Lett.* **2002**, *89*, 185901.

(32) Shi, W.; Johnson, J. K. *Phys. Rev. Lett.* **2003**, *91*, 015504.

(33) NIST Chemistry WebBook, http://webbook.nist.gov/chemistry.